Review article

Kai Braun*, Florian Laible, Otto Hauler, Xiao Wang, Anlian Pan, Monika Fleischer and Alfred J. Meixner

Active optical antennas driven by inelastic electron tunneling

https://doi.org/10.1515/nanoph-2018-0080
Received July 2, 2018; revised July 26, 2018; accepted July 28, 2018

Abstract: In this review, we focus on the experimental demonstration of enhanced emission from single plasmonic tunneling junctions consisting of coupled nano antennas or noble metal tips on metallic substrates in scanning tunneling microscopy. Electromagnetic coupling between resonant plasmonic oscillations of two closely spaced noble metal particles leads to a strongly enhanced optical near field in the gap between. Electron beam lithography or wet chemical synthesis enables accurate control of the shape, aspect ratio, and gap size of the structures, which determines the spectral shape, position, and width of the plasmonic resonances. Many emerging nano-photonic technologies depend on the careful control of such localized resonances, including optical nano antennas for high-sensitivity sensors, nanoscale control of active devices, and improved photovoltaic devices. The results discussed here show how optical enhancement inside the plasmonic cavity can be further increased by a stronger localization via tunneling. Inelastic electron tunneling emission from a plasmonic junction allows for new analytical applications. Furthermore, the reviewed concepts represent the basis for novel ultra-small, fast, optically, and electronically switchable devices and could find applications in high-speed signal processing and optical telecommunications.

Keywords: optical antennas; inelastic electron tunneling; hot electrons.

***Corresponding author: Kai Braun,** Institute of Physical and Theoretical Chemistry, Eberhard Karls University Tübingen, Auf der Morgenstelle 18, 72076 Tübingen, Germany; and Center for Light-Matter-Interaction, Sensors and Analytics LISA+, University of Tübingen, Auf der Morgenstelle 15, 72076 Tübingen, Germany, e-mail: kai.braun@uni-tuebingen.de. http://orcid.org/0000-0003-3774-0507
Florian Laible and Monika Fleischer: Institute for Applied Physics, Eberhard Karls University Tübingen, Auf der Morgenstelle 10, 72076 Tübingen, Germany; and Center for Light-Matter-Interaction, Sensors and Analytics LISA+, University of Tübingen, Auf der Morgenstelle 15, 72076 Tübingen, Germany
Otto Hauler and Alfred J. Meixner: Institute of Physical and Theoretical Chemistry, Eberhard Karls University Tübingen, Auf der Morgenstelle 18, 72076 Tübingen, Germany; and Center for Light-Matter-Interaction, Sensors and Analytics LISA+, University of Tübingen, Auf der Morgenstelle 15, 72076 Tübingen, Germany
Xiao Wang and Anlian Pan: Key Laboratory for Micro-Nano Physics and Technology of Hunan Province, School of Physics and Electronics Hunan University , Changsha 410012, China

1 Introduction

Generally, antennas are used to enhance the radiation or detection of electromagnetic waves. This also holds true for optical antennas, which are applied in the spectral region of optical frequencies [1, 2]. Adapting the concept to this regime however leads to certain limitations. At optical frequencies, metals are no longer perfect conductors, and light can penetrate the metals. High losses, resonances, etc., are the consequences. Nevertheless, these drawbacks also provide high mode confinement, and localized surface plasmon resonances (LSPRs) offer high Purcell factors with an enhanced local density of optical states [3]. Recently optical antennas have gained great attention, e.g. for focusing visible light down to a small fraction of the wavelength, far beyond the diffraction limit [4–6].

The simplest type of an optical antenna is a single noble metal nanoparticle, e.g. a gold nanosphere [7], which can efficiently convert electromagnetic waves from free space to a localized surface plasmon (LSP) [8] and create enhanced electric fields at its surface, or enhance the emission of a quantum system by transforming the near-field information into far-field radiation [9]. Furthermore, the short dephasing time of the LSP [10, 11] can additionally enhance the signal of a nearby quantum system by altering the lifetime of the excited states [8].

These effects are widely used to enhance spectroscopy response [12], photon conversion [13–15], or nonlinear effects [16–18].

However, the shape of the antenna is an important parameter. Triangles and nanorods concentrate light much more effectively than a sphere [19]. By engineering the size and the aspect ratio, the LSPR of such structures can be tuned over a wide range to adjust the antennas to the requested spectral operating window [20, 21]. Moreover, these geometries control the direction and polarization of the emitted signal [22, 23]. Even further improvement can be achieved by coupled antennas [24, 25] consisting of two or more closely spaced nanoparticles [26, 27], which leads to a strongly enhanced optical near field in the gaps between the constituents [28, 29]. The strong confinement in the gap region is extremely localized and allows for ultra-compact sources of electromagnetic radiation. The multiple particle design offers the opportunity to electrically contact the antennas as electrodes with a tunneling junction in between by directly attaching leads to the structures [30, 31]. Unfortunately, it is impossible to externally generate oscillating currents in the near-infrared or optical frequency range, so they normally cannot be directly driven by electrical generators. In most cases, these antennas are excited either by thermal or, most commonly, by light sources.

Luckily, there are some workarounds for this limitation. The most common one, already known for more than 40 years, is the use of inelastic electron tunneling (IET) in metal-insulator-metal structures (MIMs) [32, 33], where electrons transfer energy to excite an LSP mode. In the case of optical antennas with a sufficiently small gap to achieve stable tunneling, IET can excite the LSPR and thus directly drive the antenna with a DC voltage applied to the individual arms. Figure 1 shows some prominent different types of MIMs that can act as active optical antennas.

Generally, they are divided into two approaches, either the fabrication of planar or vertically arranged electrodes via lithography or MIMs created by scanning tunneling microscopy (STM), where the tip and sample act as the coupled system. Theoretically, the quantum efficiency (QE) of the electron to photon conversion in IET should be able to reach (10^{-1}) [34]. However, for many years experiments showed rather lower figures, more likely around (10^{-6}) [3]. Recently several groups have shown much higher QEs (~10^{-4}) by fabricating resonant gap antennas [31, 35] or via additional laser pumping QE (~10^{-2}) [30, 36, 37]. The complementary illumination with laser light creates a high concentration of the so-called hot electrons [38, 39]. The decay of LSPRs induces excitons with much higher energy than the thermal distribution, for which reason they are called hot carriers. These excited electrons have much longer lifetimes, up to picoseconds rather than the otherwise typical few 10 fs [39], and enable processes that are not possible with thermalized carriers [39]. Section 2 introduces different kinds of antennas from single to coupled types and describes the effect of IET and how to generate high-frequency currents with a DC voltage to drive the antennas. Section 3 shows major approaches for experimentally producing and measuring small gap antennas. Section 4 finally describes the role of additional laser pumping to create a high concentration of hot carriers and their influence on IET.

2 Physical concepts

2.1 Optical antenna

The high concentration of free charge carriers in noble metals gives rise to high plasma frequencies, such that

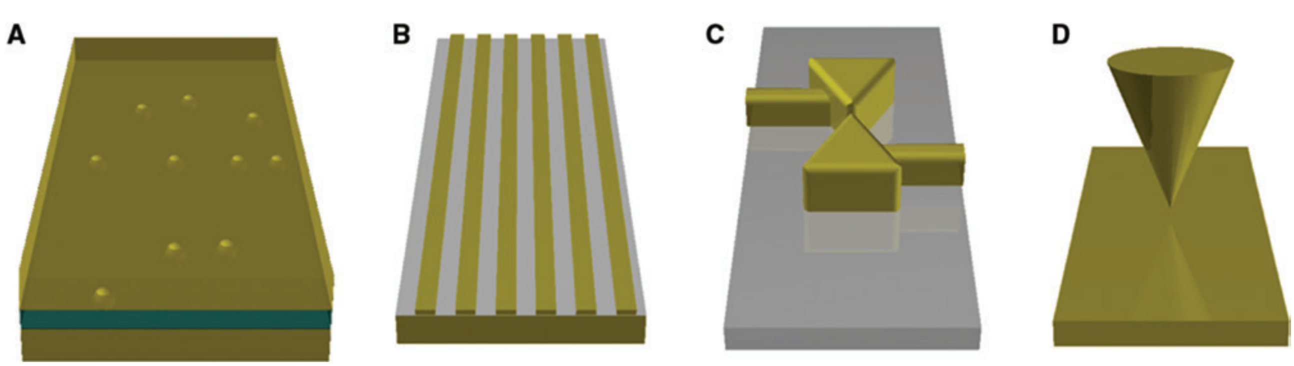

Figure 1: Sketch of various MIM structures, where a LSPR mode can be excited by IET.
(A, B) Au substrate coated with a thin insulating layer (~1 nm) with the antenna structure on top. (A) Spin-coated nanoparticles partially embedded in a polymer and top gated by an additional conducting layer, e.g. an evaporated gold film. (B) Lithographically etched wires. (C) Planar antenna structure on insulating substrate with sufficiently small gap. (D) Noble metal STM tip above a noble metal substrate.

they can support surface plasmon polariton modes [40]. On metal-dielectric interfaces, these can travel over distances of multiple wavelengths [41]. Surface plasmon polaritons can be scattered or guided by edges or by constrictions and therefore be confined to small locations/ dimensions generating a LSP [42]. In small metallic structures, the band structure differs from that of the bulk material. Instead, the bands show discrete states that have certain resonances at specific wavelengths and create LSPR modes, which depend on the material and on the dimensions of the confined space. The localized plasmon modes gives rise to the strong enhancement of electric fields on rough noble metal films and have been used in surface-enhanced Raman spectroscopy [12]. The protrusions in these films act as local emitters and increase the excitation of molecules. High roughness increases the chance that two or even more tips are in close vicinity and form a coupled LSPR or hot spot, which shows the highest enhancement within the small gap between them and enables single molecule detection [28]. Another prominent route to fabricating plasmonic particles is wet chemical synthesis [43, 44]. Various routines have been developed to grow particles with many different shapes such as spheres, rods, and triangles [45–47] or multiple protrusion particles like stars [48]. However, rough island films are difficult to reproduce, and both the films and the colloidal particles offer limited control over the specific localization and the desired plasmon resonance wavelength.

The basic function of an antenna is to transmit or receive information transported by electromagnetic waves [49]. For an optical antenna, the first step is the localization of radiation to a quantum system like a molecule. The size of the quantum emitter is small compared with the wavelength of light. This mismatch lowers the efficiency of excitation and the radiation of the quantum system but can be improved by coupling to an antenna. A simple antenna structure to reduce the mismatch and bridge the size difference is a $\lambda/2$ antenna in the shape of a nanorod where the length determines the resonance wavelength. However, the penetration of light into metals introduces delays between the driving electric field and the free electrons, resulting in a resonance for lengths that are effectively shorter than the $\lambda/2$ condition by a factor of 2–5 [50]. Nevertheless, the interaction of quantum systems with optical radiation is greatly improved, when coupled to such an antenna. Electron or ion beam lithography can produce structures with a precision well below 10 nm, making them ideal tools for producing individual optical antennas. Over the last few decades, several different antenna types have been proposed and produced, of which Figure 2 shows a non-exhaustive overview.

A more advanced function of optical antennas is to manipulate the direction of the radiated power. A simple rod antenna has a dipolar emission profile. For simply enhancing signals to increase the information depth or to increase the excitation probability of quantum systems, this may be sufficient. For more complex functions, however, e.g. integration in electronic circuits, a more sophisticated control is required. A dipole will radiate into a large solid angle and hence even to unwanted directions, which can introduce cross talk with other functions. A prominent antenna configuration with a specific radiation direction and good control of the polarization

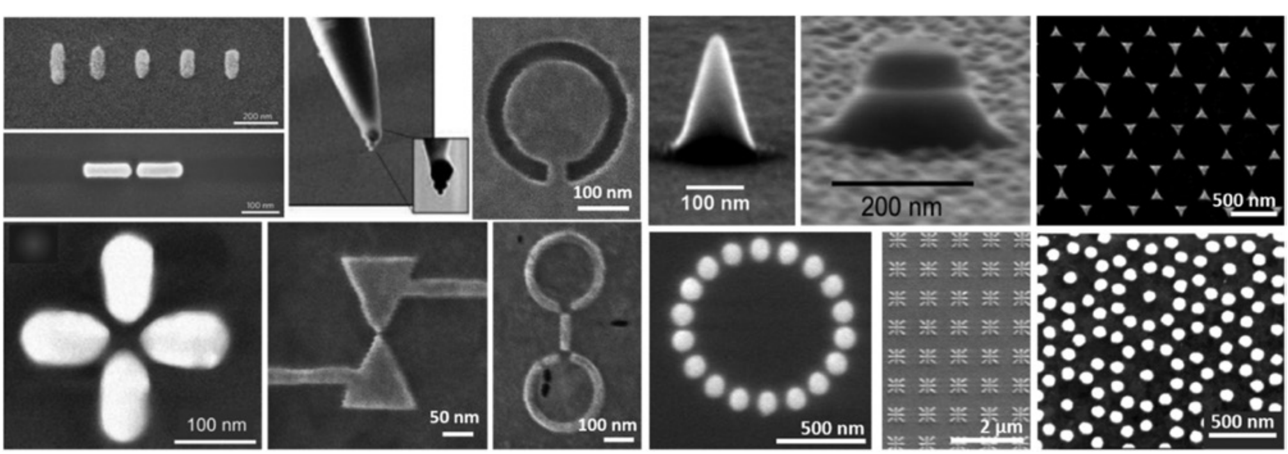

Figure 2: Clockwise from top left: Yagi-Uda antenna from Ref. [22] reprinted with permission from AAAS, a glass fiber tip with attached noble metal nanoparticles reprinted from Ref. [51], negative splitring, gold cone on substrate [52], vertical dimer gold-Al_2O_3-gold [52], gold nanotriangles prepared by nanosphere lithography [52], gold nanodiscs in quasicrystalline order [52], star-shaped gold nanoantennas [52], corral shape made from gold nanoparticles [52], two coupled splitrings, connected bowtie antenna, cross antenna [26], and coupled $\lambda/2$ antenna.

is a Yagi-Uda antenna [53] [see Figure 2 (top left)], which works also in the optical regime. However, this design is rather complex to fabricate with nanometer dimensions and additionally relatively big in size. Non-symmetrically aligned coupled antennas or statistically structured junctions [30] achieved by electromigration or cracks in gold wires show also reasonable directionality of radiation and are much simpler to fabricate.

Optical antennas are typically used to enhance the radiation of quantum emitters coupled to the antenna. In the case of an active antenna, an additional function is implemented. Here we present a review on active antennas where the emitted signal is produced in the structure itself by an external DC electrical field causing IET. This can be achieved either by designing the antenna such that the driving force from IET couples to a radiative LSPR mode [31, 35, 37] or by introducing artificially generated quantum states in the antenna by a functional coating with molecules on the antenna surface [36].

2.2 Coupled optical antennas

The electromagnetic enhancement by an LSPR is the major benefit of an optical antenna. The highest enhancements can be reached by coupled antennas, where the strongest fields are generated within the gaps separating them. One of the simplest, nevertheless, often used types is the end-to-end coupling of two effective $\lambda/2$ rod antennas. The LSPR of such systems can rather easily be engineered, and their optical properties can be predicted by simulations [54]. The antenna behaves like a coupled dipole and thus has two fundamental eigenmodes, a lower energy bright and a higher energy dark mode. The radiation rate of the dark mode is greatly supressed; therefore, mostly the bright mode is of interest for active antennas. The coupling strength increases with decreasing gap sizes, and the energy splitting between the two modes increases, shifting the bright mode to lower frequencies. The electric field enhancement scales with the coupling strength and gaps smaller than a few nanometers show a nonlinear increase in enhancement [25, 55], making them also suitable for tunneling junctions. However, with gaps smaller than about half a nanometer [56], the quantum limit is reached, and the antennas cannot be treated anymore as two isolated particles, resulting in a breakdown of the hot-spot in the center. Over the past few years, many different variations of coupled systems have been fabricated and tested with a particular focus on quantum mechanical effects in plasmonic structures featuring subnanometer gaps [57]. Probably the most prominent type of a gap antenna is the so-called bowtie antenna, which was also one of the first structures proposed as an optical antenna [58]. Nevertheless, there appeared to be only little differences in the enhancement factors of different dimer structures showing the same resonance wavelength, and the overall dominating factor is the interparticle distance. Still, controllably fabricating gaps of few nanometers down to subnanometers between individual nanostructures remains a major bottleneck in the investigation of coupled optical antennas. By using top-down approaches such as electron beam lithography or focused ion beam milling, gaps of few nanometers can be fabricated [59, 60], but for even smaller gaps, one often needs to rely on statistics or add additional measures such as flexible substrates or thermal reshaping [61, 62]. With the novel development of focused helium ion beam milling, the direct cutting of sub-5 nm gaps has come within reach [63, 64]. Extremely narrow gaps can be achieved, e.g. by electromigration or using break junctions [65–68]; however, these techniques result in random shapes in the gap area. Another possibility is the controlled photochemical growth of gap antennas [69] or electroless deposition onto particles, e.g. prepared by micellar lithography [70], thus increasing the size of neighboring particles in order to decrease the gap size. Alternatively, dielectric spacer layers can be introduced between the antenna parts. Here atomic layer depositions offer excellent control over the thickness of conformally deposited oxide layers down to single atomic monolayers, which is particularly useful for vertical configurations [71], but have also been demonstrated to create lateral nanometer gaps [72, 73]. The oxide can subsequently be etched away to create vertical air gaps [74]. Finally, molecular spacers such as self-assembled monolayers or short DNA strands offer just the right length scale for maintaining nanometer gaps. Such systems have been employed in different configurations, from binding pairs of nanoparticles [75–78] to creating subnanometer gaps between metal layers and dispersed nanoparticles [79]. Alternatively, ultra-narrow gaps may be achieved by attaching the nanostructures to feedback controlled movable probe tips for sensitive gradual approach down to contact [56].

For active antennas, an additional requirement needs to be fulfilled. The single antenna arm must be connected by strip lines as electrodes to apply the DC bias voltage. The attached metallic/conducting strip lines can interfere with the LSPR of the antenna arm and cause a perturbation decreasing the enhancement factor. To alleviate this difficulty, simulations and experiments show that leads that are connected at nodes of the electric field have a negligible influence on the antennas [80].

Alternatively, a gap antenna can also be created by a noble metal tip that is approached to a noble metal substrate, an assembly well known from tip-enhanced Raman spectroscopy [5, 81]. The sharp metal tip can be modeled as a point dipole. At distances smaller than a few nanometers to a noble metal, this charge creates a mirror dipole in the sample surface, creating a gap mode like a coupled antenna [82, 83]. Instead of a flat surface, the tip can also be coupled with lithographically produced metal structures or nanoparticles [55]. This arrangement represents a vertical antenna with an excellent gap distance control. Recent experiments have shown that gap mode microscopy can have single molecule Raman sensitivity, showing comparable enhancement factors to the lithographically produced structures. Additionally, the hot spot of this antenna can be localized to an area smaller than a single nanometer [84]. To keep the tip near the surface, a feedback mode is required. This can be based either on atomic forces or on tunneling. The latter gives direct access to a vertical active optical antenna, as electric leads for the tip and the substrate are already integrated.

2.3 Inelastic electron tunneling

Tunneling junctions have been produced in various configurations. They are constructed as layered MIM sandwiches, flat metal surface-insulator-nanoparticles, or by STM. They all have in common that electrons experience a potential barrier when tunneling from one side to the other. Without an applied bias voltage and with both arms at the same potential, electrons are exchanged across the contact potential until the Fermi levels of the electrodes are equalized. By applying a potential difference between the contacts, a constant tunneling current can be generated. The number of electrons reflects the current, which can vary drastically from a few hundred picoamperes to several tens of microamperes depending on the applied bias voltage, material and the size of the junction. The largest impact by far is imparted by the metal to metal distance. Typically, electrons tunnel elastically (Figure 3), and no energy is transferred to the surroundings. At a fixed distance and bias voltage, the elastic tunneling rate is only determined by the joint local density of states (LDOS) of the tip and the sample. By keeping the distance constant and sweeping the bias voltage, mapping of the LDOS is possible by recording a dI/dV curve, called scanning tunneling spectroscopy.

However, the potential barrier in the tunneling junction represents a Schottky barrier, and quantum particles like electrons may either be reflected or transmitted at the junction, leading to quantum shot noise [85]. The frequency of the noise scales with the applied bias voltage. To generate shot noise with optical frequencies, the bias needs to be around 2 eV (Figure 3), as the energy of the bias voltage sets the energy limit for linear electron scattering processes. Then, an inelastically scattered electron can couple to a LSPR mode in the junction that decays radiatively. In distinct single gold or silver atom contacts, additionally some nonlinear processes become accessible [86], which will not be discussed further here.

3 Experimental approach

In this section, we will focus on the most frequently used distinct methods to achieve active optical antennas driven by IET. Over the last two decades, the localized excitation

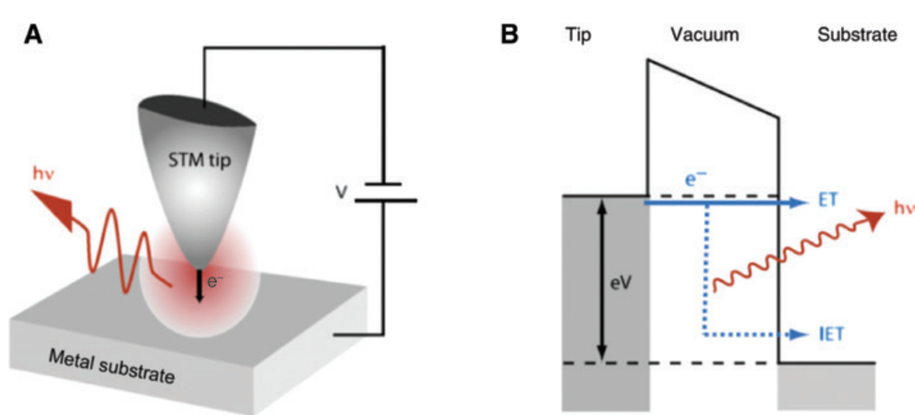

Figure 3: Illustration of the electrical excitation process by tunneling electrons.
(A) The tunneling current in an STM can be used as a nanosource to generate light from the tunnel junction. (B) Schematic potential energy diagram illustrating the mechanism for photon emission in an STM junction. Elastic (ET) and inelastic tunneling (IET) processes are indicated. IET excites a LSP between tip and sample. The photons emitted during the radiative decay of the plasmon are detected in the far field, reprinted from Ref. [3] copyright (2010), with permission from Elsevier.

of various systems like metal or molecular island films, single molecules, and metallic structures via IET has been extensively studied by light emission from a STM tunneling junction. These experiments offer precise control of the localization and gap distances, while the current feedback stabilizes the junction. Conversely, this arrangement is not suited to be integrated in an electronic circuit. In the past 5 years, several groups started to prepare active optical antennas on a chip. Improved electron and ion beam lithography gives rise to structures with small gap sizes, which can be modified to acquire stable tunneling junctions. An often-used approach is electromigration. Here an electric field is applied to wires or junctions to migrate atoms in a favorable direction and create tunneling junctions or even single atom contacts or switches.

3.1 Scanning tunneling microscopy

Typically, platinum-iridium (Pt/Ir) or tungsten (W) tips are used in STM experiments. These metals offer high stiffness and stability. The first STM light emission experiments were performed with W tips on gold surfaces, showing radiative recombination via LSPRs [87] in the sample. However, the dielectric functions of W and Pt/Ir differ strongly from those of pure noble metals. Only several materials like gold, silver, copper, aluminium, or some metal nitrides possess sufficiently high concentrations of free electrons to exhibit a LSPR in the optical regime [88]. Therefore, later IET experiments were performed with Au and Ag tips, which form coupled resonant antennas and showed much higher light emission by a factor of more than 10 [89]. As discussed previously, for an antenna, the shape and aspect ratio also determine the resonance frequencies of the LSP. While the basic shapes of the tips are rather similar, the radius of the apex and the opening angle can differ considerably and have strong influence on the resulting IET spectra. Several calculations and experiments proved that a larger opening angle shifts the resonance to higher energies and larger radii of curvature of the apex increase the intensity [90]. Additionally, truncated tips and tips with a very large apex often show multiple peaks, which depend on the size and shape of the tip [91, 92]. For active optical antennas, tips that show a single band in the desired frequency range are especially of interest.

The bandwidth of the antennas is determined by the plasmon resonances, while the intensity can also be modified by the joint LDOS of the junction. This was nicely demonstrated by designing small atom chains [93, 94] or islands [95]. Silver atom chains were fabricated on a NiAl (110) substrate by field emission of the Ag tip. The one-dimensional structure consisting of 10 Ag atoms is too small to show plasmonic features, which could be proven by IET. The spectra taken above the chain show the same spectral behavior as on the bare substrate. Nevertheless, the chain acts like a particle in a box, possessing several electronic states with an increasing number of nodes and antinodes for increasing energies (see Figure 4D), which could nicely be shown by dI/dV spectroscopy. The same nodes and antinodes appear when IET photon maps are recorded, by scanning the tip with different bias voltages

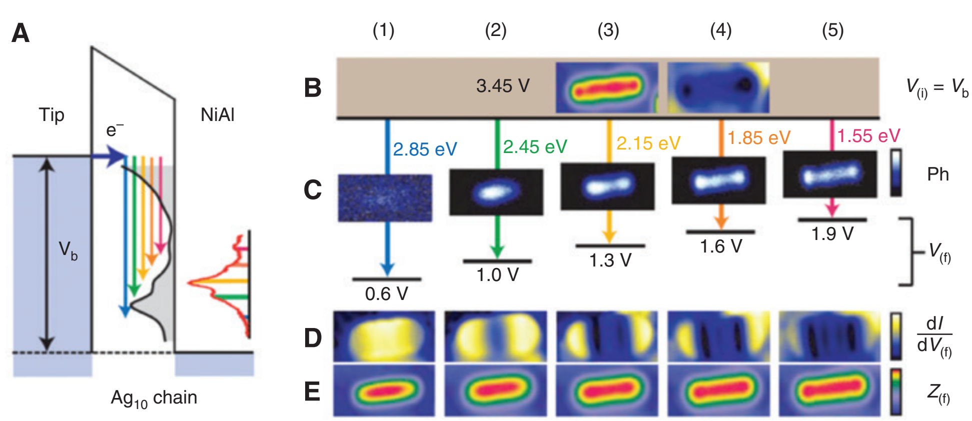

Figure 4: Spectroscopic mapping of the LDOS modification by introducing an Ag-chain in the tip sample junction.
(A) Schematic representation of radiative transitions in an Ag_{10} chain, where electrons undergo transitions between the Ag chain states (black dI/dV curve) and of the corresponding photon emission spectrum (red). Five vertical arrows of different colors show transitions into the LDOS of Ag_{10}. (B) Topography (left) and simultaneous dI/dV image at the initial state of all the transitions. (C) Photon maps for different energies of transitions between the same initial state $V_{(i)}$ to five different final states at $V_{(f)}$. The photon images show zero to four maxima. (D) dI/dV images for the five final states showing the nodes (dark bands) for the ground state and the excited states of the particle in a box. The positions of the emission maxima in the photon maps coincide with the nodes in D. (E) Topographic images [$Z_{(f)}$] of the Ag10 chain at the respective biases, from Ref. [93] reprinted with permission from AAAS.

above the chains. Other works that recorded photon maps on Au step edges (not shown in the figure) or nano triangles show standing wave patterns [see Figure 5 (I)] at constant bias voltages.

They state that these different intensities are associated with electronic surface states altering the LDOS. Therefore, the intensity of IET is generated by two contributions, the radiative transition between the initial and final state and the coupling to the LSPR, which enhances the emission.

Another way to modify the junction has recently been shown. A short polymer chain on surface-synthesized polythiophene is picked up by a STM tip and lifted in a controlled way, but still kept in contact with the Au surface [see Figure 5 (II, right)]. Normally, the luminescence of a molecule that remains in contact with the tip or the substrate is severely quenched by the metal. However, in this configuration, the molecule in the middle of the junction is decoupled from the metal by other molecules of the chain and can be excited by IET. Interestingly, the luminescence shows a strong non-symmetric polarization dependence, which is not shown here. Nevertheless, Figure 5 (IIB, C) describes the applied model for the behavior. With a negative bias voltage at the tip, above a certain threshold, electrons from the Fermi level can be injected into the lowest unoccupied molecular orbital (LUMO) of a molecule in the chain. This electron may combine radiatively with a hole injected into the highest occupied molecular orbital (HOMO), while the gap mode of the junction enhances the signal. However, with an opposite bias voltage, the energy level of the LUMO is not accessible from the Fermi level of the sample, leading to a lower QE of the IET. Hence, the junction shows the behavior of a light emitting diode while only consisting of a few molecules and thereby a convincing example of active devices with a size below several nanometers.

3.2 Lithography and electromigration

Notwithstanding the tremendous achievements and the high level of control that were shown by means of STM junctions, for device integration simpler arrangements are needed. An interesting and increasingly used method is the fabrication of planar coupled antennas by electron or ion beam lithography. Although these methods have increased in accuracy and resolution and show nanometer precision, the engineering of a gap between two antenna arms smaller than a few nanometers is challenging. However, effective IET is only possible with a gap size smaller than about a nanometer. To combine the lithographic control over the antenna shape and aspect ratio with sufficiently small gap sizes, various approaches have been introduced.

A recently presented study utilized monodisperse gold nanospheres covered with a ligand shell to introduce a double barrier tunneling junction in the gap of tailor-made contacted $\lambda/2$ antennas. An atomic force microscope

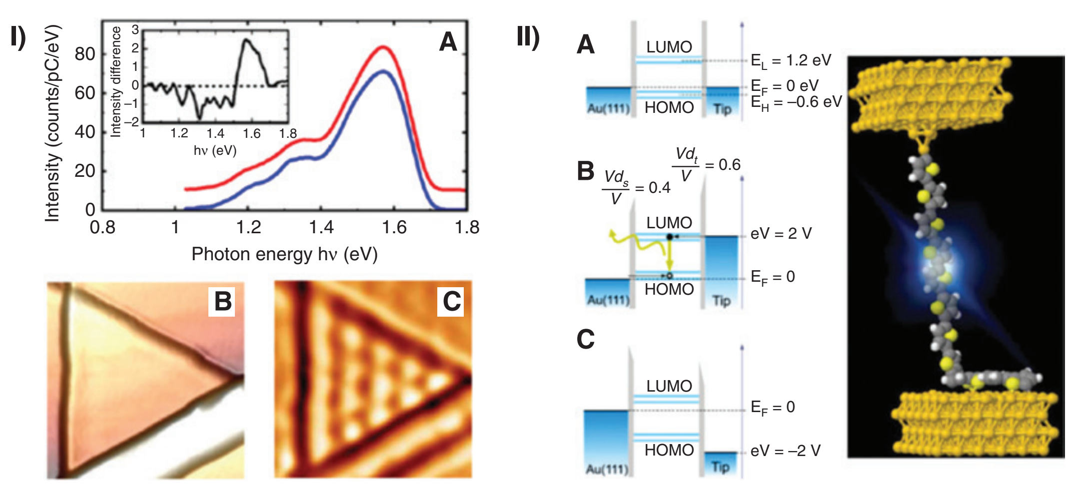

Figure 5: Modification of the IET light emission by a structure and a single molecule.
I. (A) Spectra of STM-induced light emission from Au(111) obtained at two locations of a triangular island (B). The inset shows the difference between the spectra. (B) Constant-current STM image of a triangular island on Au(111). (C) Energy-resolved (1.65 eV < E < 1.7 eV) photon map acquired simultaneously with the STM image in B, taken with permission from [95]. II. Artistic image of the polymer junction and sketch of the band structure of the polymer junction representing the energies of the HOMO and LUMO states at (A) zero bias voltage. At a high negative sample voltage (B), the HOMO is shifted above the Fermi level of the sample and the LUMO below the Fermi level of the tip. Electrons injected from the tip into the LUMO can radiatively decay into the partially emptied HOMO. For inverse bias (C), the LUMO remains above the Fermi level of the sample, and no intramolecular radiative transition occurs, taken with permission from [96].

was used to push the spheres to the desired position in the gap and form electrically driven optical antennas. The antenna structures were top-down fabricated by focused ion beam lithography from single crystalline gold flakes, with gap sizes around the particle size. When a sufficiently high bias voltage is applied, the junctions emit light with a dipolar radiation pattern. The position and size of the particle have a strong influence on the achievable QE and the resonance frequency [see Figure 6 (I)]. Additionally, the authors constructed an equivalent gap in a strip line of the same thickness and width using the same kind of sphere, which showed no resonance in the optical regime and an order of magnitude lower QE to prove the enhancement of the antenna. Recently, the authors also produced optical Yagi-Uda antennas with a tunneling feed [97].

Despite the impressive results, pushing single particles to each desired position is time-consuming and ineffective for large-scale on-chip preparation. Another prominent way to produce two-dimensional tunneling junctions is the use of atom migration along an applied electric field. The junction in Figure 6 (II) was fabricated from a gold nanowire by Joule heating [30] triggered by a voltage applied to the two ends of the wire. In the process, an electrically induced constriction appears as the wire gets electrically thinned and the monitored conductance drops until a tunneling junction is formed [Figure 6 (IIA)]. These junctions also nicely show IET-driven luminescence, which increases in intensity and blue shifts under an increased bias voltage. Nevertheless, antennas produced with this method offer poor control over the LSPR and the directivity of the emission pattern.

Consequently, in the latest results shown here (see Figure 7), both methods were combined. The basic antenna configuration was fabricated by electron beam lithography where the electric connection leads are again placed at the calculated nodes of the electric field to minimize the perturbance of the antennas' LSPRs. Between the designated single antenna arms, a nano-constriction is implemented, which again can be transformed into a tunneling junction by successive electronically induced atom migration. In contrast to the previously shown experiment with the sphere connected to the active antennas, here an angle is introduced in the plane of the connected single

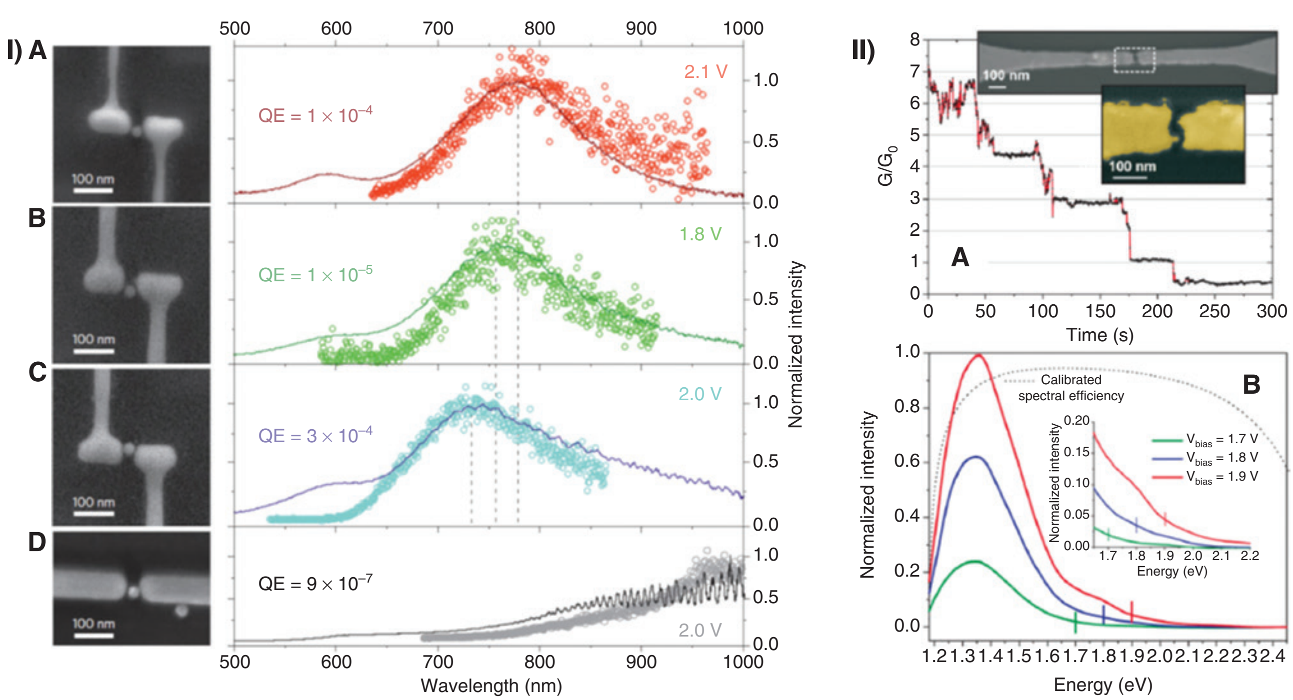

Figure 6: On-chip solutions for planar tunneling junctions.
I. Electroluminescence (open circles) and scattering spectra (solid lines) for different antenna geometries (A–C) and a non-resonant wire several micrometers long (D). The external QEs and applied voltages are stated. The left column shows electron micrographs of the corresponding structures reprinted with permission from Ref. [31] copyright 2015 Springer Nature. II(A). Normalized conductance during the last moments of the electromigration process showing quantum conductance steps. Inset: Scanning electron micrograph of an Au nanowire after electromigration and close-up view of the junction area. (B) Emission spectra showing the shift with the applied bias. The vertical bars indicate the quantum limit. Inset: Magnified energy distributions near the quantum limit, reprinted with permission from Ref. [30], copyright (2015) American Chemical Society.

arms, which forms a V-shape of the coupled arms. When these antennas are activated by IET, the V-shape leads to a unidirectional emission pattern with a maximum directivity of 5 dB (see Figure 7, bottom). The directivity can be tuned either passively via the angle between the antenna arms or actively by the applied bias voltage. These experiments demonstrate promising on-chip optical transmitters, which emit photons induced by an applied electrical signal.

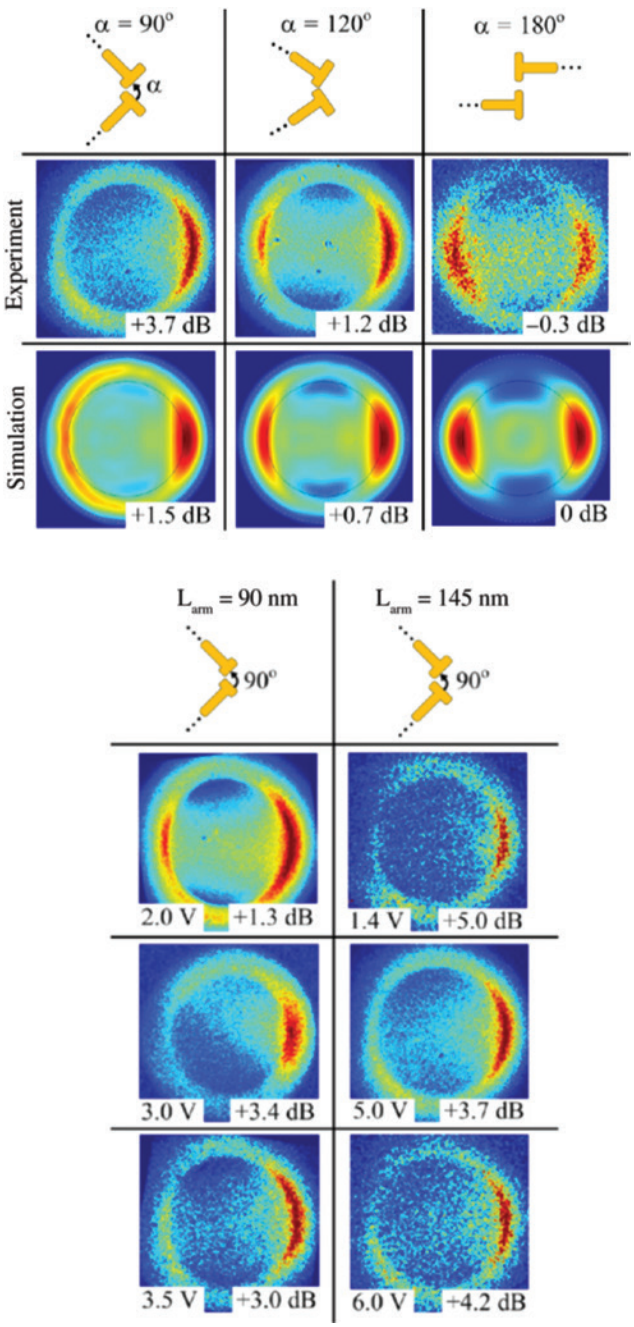

Figure 7: (Upper panel) Evolution of the directivity with the opening angle of a V-antenna.
Experimental back-focal plane images and the corresponding simulated patterns are shown for three different angles. (Lower panel) Experimental full-spectrum back-focal plane images depicting the evolution of the directivity with bias voltage for two V-antenna geometries, reprinted with permission from Ref. [35], copyright (2017) American Chemical Society.

4 Inelastic electron tunneling and additional laser illumination

Despite the amazing results shown with purely IET-driven optical antennas, most investigations on optical antennas have been carried out under laser illumination. Within the last decade, there has been a tremendously increased interest in laser-induced hot carrier creation. Their role in plasmonic systems is discussed for various applications in catalysis and enhanced sensitivity and emission. Consequently, these hot carriers can also have a strong influence on tunneling-induced light emission from gap antennas. So far, experiments with IET-driven antennas that are additionally laser illuminated have only been undertaken in STM configuration. Nevertheless, these studies show a strong increase of radiative electron-hole recombination in optically pumped tunneling junctions, which cannot simply be explained by an additive superposition of both effects (light and IET excitation). The experiments were carried out on bare gold junctions [37] and on metal-molecule-insulator-metal contacts [36], where the molecule introduces additional surface states.

On bare contacts, the IET emission follows nicely the results of earlier studies as described in Section 3.1. The tips used in this experiment have large apexes and support three LSPR modes, which is in good agreement with theory (see Figure 8A, solid green circles).

The QE is estimated to about 10^{-5}, which is rather high for the STM configuration and most likely owing to the large apex. For a junction illuminated at 633 nm and a low bias voltage, the IET excited LSPR modes are not present. However, an additional band appears, which is associated with optically excited radiative electron-hole recombination in gold and well known from tip-enhanced Raman spectroscopy with gold tips [98, 99]. The luminescence of gold is approximately five times higher than the maximum IET emission. With an increased bias above the threshold for IET, the photon flux is strongly increased (Figure 8), and the spectra again show the three LSPR modes together with electron-hole recombination, but this time, the LSPR modes show the highest luminescence. This extraordinary enhancement in the IET process is explained by radiative recombination of hot electrons, which are created by the

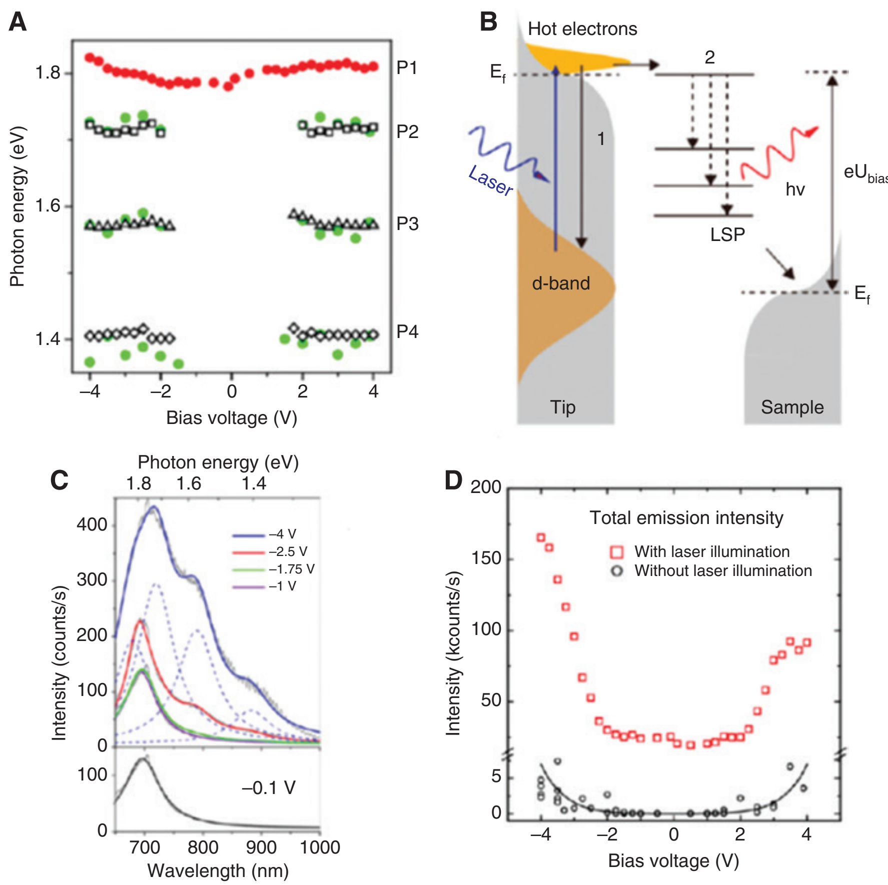

Figure 8: STM light emission spectroscopy on a bare Au-Au junction with and without additional laser pumping.
(A) Peak positions of PL bands due to laser excited electron-hole combination (P1) and IET (P2, P3, and P4, black symbols). For comparison, the three radiative LSP modes (solid green circles) excited by pure IET in the junction without laser illumination are plotted as well. (B) Sketch of the processes involved in a biased Au-Au junction under laser illumination. Process (1) is related to electron-hole recombination and radiative inelastic plasmon relaxation. Process (2) is related to the radiative decay of LSP modes created by IET (C) PL spectra (gray lines) and the fitting curves (solid smooth lines) of the laser illuminated Au-Au junction. At low bias voltages $|U|$ <1.75 V, the spectral line shape consists of one band. As the negative bias voltage increases, LSPR modes appear. (D) Comparison of the spectrally integrated total PL intensities as a function of bias voltage from the irradiated Au-Au junction (open red squares) and from the non-irradiated junction (open circles), reprinted with permission from Ref. [37], copyright (2015) American Chemical Society.

incident laser beam (Figure 8B). The increased lifetime of these hot carriers gives rise to a much higher radiative recombination rate via the LSPR modes.

In a second experiment, the STM junction was modified by introducing a self-assembled monolayer (SAM) on the gold substrate. The molecules of the self-assembled monolayer are chemisorbed on the sample. This way the HOMO of the chemically bound molecule forms an additional hybrid surface state, which was confirmed by X-ray photon spectroscopy. The pure IET excitation shows a similar behavior as the previously discussed lifted polymer chain (see Figure 9). The luminescence is strongly bias polarization dependent with a low number of photons emitted at a negative bias at the tip, while a positive bias shows a 25 times higher photon flux with a QE of about 10^{-5}, analogous to a light emitting diode. Under a sufficiently high positive bias, the tip injects holes into the HOMO of the surface state, which can radiatively recombine with an electron from the Fermi level of the sample. The single emission band nicely shows that the tip in this experiment was very sharp. However, when this junction is illuminated again with a 633 nm laser, the photon emission is even further increased and reaches a QE of almost 1%. Power-dependent spectroscopy reveals a nonlinear increase of the emission (see Figure 9D) with an accompanied bandwidth narrowing, which implies a stimulated emission process.

This extreme enhancement is mainly given by the depletion of the HOMO of the surface-bound molecule via hole injection, while the laser-driven generation of hot electrons close to the Fermi level creates an inversion population (see Figure 9C). The strongest enhanced

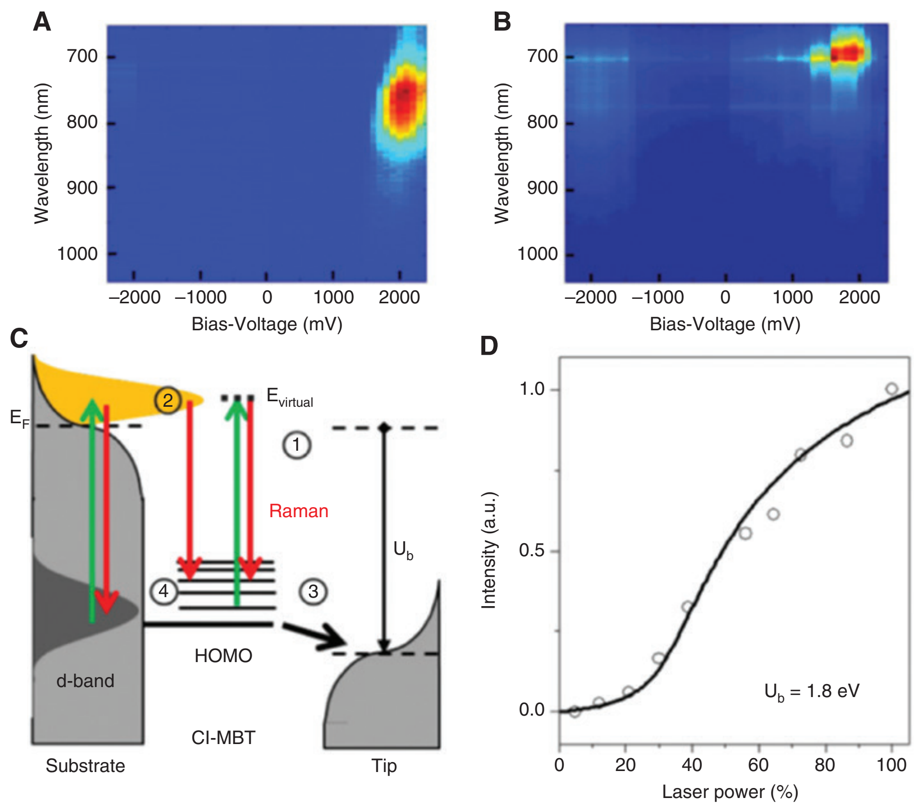

Figure 9: Superluminescence from a laser pumped molecular tunneling junction.
(A) Electroluminescence spectra excited by inelastic tunneling without laser illumination as a function of the bias voltage. (B) Spectra from the tunneling junction excited at $\lambda = 632.8$ nm as a function of the bias voltage. (C) Schematic energy level diagram of the gap/molecule hybrid system in a laser-illuminated tunneling junction with (1) Raman scattering of the molecule, (2) hot electron generation, (3) HOMO depletion by hole injection and (4) stimulated emission. (D) Normalized experimental data (open circles) and calculated total emission (solid line) as a function of the incident laser power for fixed bias voltage 1.8 eV revealing a nonlinear increase, taken with permission from [36].

Raman emission from the molecule then acts as an optical seed for stimulated emission in the cavity formed by the tip and sample and creates superluminescent radiation. This effect shows the concept on how optical enhancement can be even further increased.

5 Conclusion

In this review, different types of active optical antennas are discussed. All reviewed antennas are activated by inelastic tunneling with an intrinsic tunneling junction. We discussed several electrically connected planar gap types and compared them to metal tips used in STM configuration. The antennas have possible applications in the field of electronic and photonic hybrid circuitry. Compared with semiconductor structures, where the spontaneous recombination rate limits the bandwidth, devices built on inelastic tunneling are only restricted by the device capacitance and the ohmic resistance of its leads, which are both quite small. Hence, bandwidths up to the terahertz regime should be reachable [100], and photon-triggered tunneling might be utilized for optical transistor operation [101]. For large-scale or on-chip implementations, it will be necessary to improve the design and the fabrication processes to increase the directivity and QE of possible devices. The QE is divided in the inelastic tunneling efficiency and the antenna efficiency. The later one may be improved by other antenna geometries with higher field enhancement in the gap, while the efficiency of inelastic tunneling is predicted to reach as high as 10% in the direct tunneling regime. The tunneling barrier height in all reviewed light-emission experiments has the same magnitude as the used bias voltages, which increases elastic tunneling to the vacuum level. The precise geometry of the junction and the gap material strongly manipulates the tunneling barrier, where for an optimized tunnel junction a device operation in the direct tunneling regime can be imagined. Therefore, cross-conjugated molecules in the gap can be utilized in engineer the tunnel barrier, while other types of molecules allow for additional conduction channels to increase the amplitude of the current noise and further increase the QE by enhancing the inelastic tunneling rate. Additional illumination can be used to excite hot electrons, which allows for additional processes such as stimulated emission and could also increase the efficiency.

Acknowledgments: Financial support of the DFG grants BR532/1-1 and FL670/7-1 and the Open Access Publishing Fund of University of Tübingen are gratefully acknowledged.

References

[1] Novotny L, van Hulst N. Antennas for light. Nat Photonics 2011;5:83–90.
[2] Fumeaux C, Alda J, Boreman GD. Lithographic antennas at visible frequencies. Opt Lett 1999;24:1629–31.
[3] Rossel F, Pivetta M, Schneider WD. Luminescence experiments on supported molecules with the scanning tunneling microscope. Surf Sci Rep 2010;65:129–44.
[4] Nerkararyan KV. Superfocusing of a surface polariton in a wedge-like structure. Phys Lett A 1997;237:103–5.
[5] Stöckle RM, Suh VD, Deckert V, Zenobi R. Nanoscale chemical analysis by tip-enhanced Raman spectroscopy. Chem Phys Lett 2000;318:131–6.
[6] Takahara J, Yamagishi S, Taki H, Morimoto A, Kobayashi T. Guiding of a one-dimensional optical beam with nanometer diameter. Opt Lett 1997;22:475–7.
[7] Fu Y, Zhang J, Lakowicz JR. Plasmonic enhancement of single-molecule fluorescence near a silver nanoparticle. J Fluoresc 2007;17:811–6.
[8] Kühn S, Håkanson U, Rogobete L, Sandoghdar V. Enhancement of single-molecule fluorescence using a gold nanoparticle as an optical nanoantenna. Phys Rev Lett 2006;97:017402.
[9] Akimov AV, Mukherjee A, Yu CL, et al. Generation of single optical plasmons in metallic nanowires coupled to quantum dots. Nature 2007;450:402–6.
[10] Sönnichsen C, Franzl T, Wilk T, et al. Drastic reduction of plasmon damping in gold nanorods. Phys Rev Lett 2002;88:077402.
[11] Konrad A, Wackenhut F, Hussels M, Meixner AJ, Brecht M. Temperature dependent luminescence and dephasing of gold nanorods. J Phys Chem C 2013;117:21476–82.
[12] Fleischmann M, Hendra PJ, McQuillan AJ. Raman spectra of pyridine adsorbed at a silver electrode. Chem Phys Lett 1974;26:163–6.
[13] McFarland EW, Tang J. A photovoltaic device structure based on internal electron emission. Nature 2003;421:616–8.
[14] Knight MW, Sobhani H, Nordlander P, Halas NJ. Photodetection with active optical antennas. Science 2011;332:702–4.
[15] Fang Z, Liu Z, Wang Y, Ajayan PM, Nordlander P, Halas NJ. Graphene-antenna sandwich photodetector. Nano Lett 2012;12:3808–13.
[16] Chen CK, de Castro ARB, Shen YR. Surface-enhanced second-harmonic generation. Phys Rev Lett 1981;46:145–8.
[17] Dadap JI, Shan J, Eisenthal KB, Heinz TF. Second-harmonic Rayleigh scattering from a sphere of centrosymmetric material. Phys Rev Lett 1999;83:4045–8.
[18] Horneber A, Braun K, Rogalski J, Leiderer P, Meixner AJ, Zhang D. Nonlinear optical imaging of single plasmonic nanoparticles with 30 nm resolution. Phys Chem Chem Phys 2015;17:21288–93.
[19] Hao E, Schatz GC. Electromagnetic fields around silver nanoparticles and dimers. J Chem Phys 2004;120:357–66.
[20] Kelly KL, Coronado E, Zhao LL, Schatz GC. The optical properties of metal nanoparticles: the influence of size, shape, and dielectric environment. J Phys Chem B 2003;107:668–77.
[21] Wackenhut F, Failla AV, Meixner AJ. Multicolor microscopy and spectroscopy reveals the physics of the one-photon luminescence in gold nanorods. J Phys Chem C 2013;117:17870–7.
[22] Curto AG, Volpe G, Taminiau TH, Kreuzer MP, Quidant R, van Hulst NF. Unidirectional emission of a quantum dot coupled to a nanoantenna. Science 2010;329:930–3.
[23] Wackenhut F, Failla AV, Züchner T, Steiner M, Meixner AJ. Three-dimensional photoluminescence mapping and emission anisotropy of single gold nanorods. Appl Phys Lett 2012;100:263102.
[24] Mühlschlegel P, Eisler H-J, Martin OJF, Hecht B, Pohl DW. Resonant optical antennas. Science 2005;308:1607–9.
[25] Schuck PJ, Fromm DP, Sundaramurthy A, Kino GS, Moerner WE. Improving the mismatch between light and nanoscale objects with gold bowtie nanoantennas. Phys Rev Lett 2005;94:017402.
[26] Biagioni P, Savoini M, Huang J-S, Duò L, Finazzi M, Hecht B. Near-field polarization shaping by a near-resonant plasmonic cross antenna. Phys Rev B 2009;80:153409.
[27] Javier A, Rico-García JM, López-Alonso JM, Boreman G. Optical antennas for nano-photonic applications. Nanotechnology 2005;16:S230.
[28] Kneipp K, Wang Y, Kneipp H, et al. Single molecule detection using surface-enhanced Raman scattering (SERS). Phys Rev Lett 1997;78:1667–70.
[29] Markel VA, Shalaev VM, Zhang P, et al. Near-field optical spectroscopy of individual surface-plasmon modes in colloid clusters. Phys Rev B 1999;59:10903–9.
[30] Buret M, Uskov AV, Dellinger J, et al. Spontaneous hot-electron light emission from electron-fed optical antennas. Nano Lett 2015;15:5811–8.
[31] Kern J, Kullock R, Prangsma J, Emmerling M, Kamp M, Hecht B. Electrically driven optical antennas. Nat Photonics 2015;9:582.
[32] Berndt R, Gimzewski JK, Johansson P. Inelastic tunneling excitation of tip-induced plasmon modes on noble-metal surfaces. Phys Rev Lett 1991;67:3796–9.
[33] Lambe J, McCarthy SL. Light Emission from inelastic electron tunneling. Phys Rev Lett 1976;37:923–5.
[34] Davis LC. Theory of surface-plasmon excitation in metal-insulator-metal tunnel junctions. Phys Rev B 1977;16:2482–90.
[35] Gurunarayanan SP, Verellen N, Zharinov VS, et al. Electrically driven unidirectional optical nanoantennas. Nano Lett 2017;17:7433–9.
[36] Braun K, Wang X, Kern AM, et al. Superluminescence from an optically pumped molecular tunneling junction by injection

of plasmon induced hot electrons. Beilstein J Nanotechnol 2015;6:1100–6.
[37] Wang X, Braun K, Zhang D, et al. Enhancement of radiative plasmon decay by hot electron tunneling. ACS Nano 2015;9:8176–83.
[38] Marchuk K, Willets KA. Localized surface plasmons and hot electrons. Chem Phys 2014;445:95–104.
[39] Narang P, Sundararaman R, Atwater Harry A. Plasmonic hot carrier dynamics in solid-state and chemical systems for energy conversion. Nanophotonics 2016;5:96.
[40] Otto A. Excitation of nonradiative surface plasma waves in silver by the method of frustrated total reflection. Z Phys A-Hadron Nucl 1968;216:398–410.
[41] Burke JJ, Stegeman GI, Tamir T. Surface-polariton-like waves guided by thin, lossy metal films. Phys Rev B 1986;33:5186–201.
[42] Novotny L, Hecht B, Pohl DW. Interference of locally excited surface plasmons. J Appl Phys 1997;81:1798–806.
[43] Sun Y, Xia Y. Shape-controlled synthesis of gold and silver nanoparticles. Science 2002;298:2176–9.
[44] Faraday M. The Bakerian Lecture. Experimental relations of gold (and other metals) to light. Philos Trans R Soc Lond 1857;147:145–81.
[45] Wiesner J, Wokaun A. Anisometric gold colloids. Preparation, characterization, and optical properties. Chem Phys Lett 1989;157:569–75.
[46] Hao E, Kelly L, Hupp JT, Schatz GC. Synthesis of silver nanodisks using polystyrene mesospheres as templates. J Am Chem Soc 2002;124:15182–3.
[47] Daniel M-C, Astruc D. Gold nanoparticles: assembly, supramolecular chemistry, quantum-size-related properties, and applications toward biology, catalysis, and nanotechnology. Chem Rev 2004;104:293–346.
[48] Jimenez de Aberasturi D, Serrano-Montes AB, Langer J, Henriksen-Lacey M, Parak WJ, Liz-Marzán LM. Surface enhanced Raman scattering encoded gold nanostars for multiplexed cell discrimination. Chem Mater 2016;28:6779–90.
[49] Fang Z, Fan L, Lin C, Zhang D, Meixner AJ, Zhu X. Plasmonic coupling of bow tie antennas with Ag nanowire. Nano Lett 2011;11:1676–80.
[50] Novotny L. Effective wavelength scaling for optical antennas. Phys Rev Lett 2007;98:266802.
[51] Höppener C, Lapin ZJ, Bharadwaj P, Novotny L. Self-similar gold-nanoparticle antennas for a cascaded enhancement of the optical field. Phys Rev Lett 2012;109:017402.
[52] Dreser C, Henken-Mellies V, Horrer A, Conti L, Blach P, Fulmes J. AG M. Fleischer Institute of Applied Physics, Eberhard Karls University Tübingen, Auf der Morgenstelle 10, 72076 Tübingen, Germany.
[53] Maksymov Ivan S, Staude I, Miroshnichenko AE, Kivshar YS. Optical Yagi-Uda nanoantennas. Nanophotonics 2012;1:65.
[54] Rechberger W, Hohenau A, Leitner A, Krenn JR, Lamprecht B, Aussenegg FR. Optical properties of two interacting gold nanoparticles. Opt Commun 2003;220:137–41.
[55] Fleischer M, Stanciu C, Stade F, et al. Three-dimensional optical antennas: nanocones in an apertureless scanning near-field microscope. Appl Phys Lett 2008;93:111114.
[56] Savage KJ, Hawkeye MM, Esteban R, Borisov AG, Aizpurua J, Baumberg JJ. Revealing the quantum regime in tunnelling plasmonics. Nature 2012;491:574.
[57] Zhu W, Esteban R, Borisov AG, et al. Quantum mechanical effects in plasmonic structures with subnanometre gaps. Nat Commun 2016;7:11495.
[58] Grober RD, Schoelkopf RJ, Prober DE. Optical antenna: towards a unity efficiency near-field optical probe. Appl Phys Lett 1997;70:1354–6.
[59] Marcel M, Trellenkamp S, Waser R, Karthäuser S. Reliable fabrication of 3 nm gaps between nanoelectrodes by electron-beam lithography. Nanotechnology 2012;23:125302.
[60] Huigao D, Hu H, Hui HK, Shen Z, Yang JKW. Free-standing sub-10 nm nanostencils for the definition of gaps in plasmonic antennas. Nanotechnology 2013;24:185301.
[61] Dickreuter S, Kern Dieter P, Fleischer M. Single particle dark-field spectroscopy of spherical dimers with down to sub-10 nm gaps fabricated by the annealing of nano-pillars. Nanophotonics 2018;7:1317.
[62] Laible F, Gollmer DA, Dickreuter S, Kern DP, Fleischer M. Continuous reversible tuning of the gap size and plasmonic coupling of bow tie nanoantennas on flexible substrates. Nanoscale 2018;10:14915–22.
[63] Olivier S, Jefimovs K, Shorubalko I, Hafner C, Sennhauser U, Bona G-L. Helium focused ion beam fabricated plasmonic antennas with sub-5 nm gaps. Nanotechnology 2013;24:395301.
[64] Wang Y, Abb M, Boden SA, Aizpurua J, de Groot CH, Muskens OL. Ultrafast nonlinear control of progressively loaded, single plasmonic nanoantennas fabricated using helium ion milling. Nano Lett 2013;13:5647–53.
[65] Taychatanapat T, Bolotin KI, Kuemmeth F, Ralph DC. Imaging electromigration during the formation of break junctions. Nano Lett 2007;7:652–6.
[66] Berthelot J, Bachelier G, Song M, et al. Silencing and enhancement of second-harmonic generation in optical gap antennas. Opt Express 2012;20:10498–508.
[67] Böhler T, Grebing J, Mayer-Gindner A, Löhneysen HV, Scheer E. Mechanically controllable break-junctions for use as electrodes for molecular electronics. Nanotechnology 2004;15:S465.
[68] Schröter U, Scheer E, Arnold R, et al. Current Transport at the atomic scale. Adv Eng Mater 2005;7:795–803.
[69] Neubrech F, Weber D, Katzmann J, et al. Infrared optical properties of nanoantenna dimers with photochemically narrowed gaps in the 5 nm regime. ACS Nano 2012;6:7326–32.
[70] Gürdal E, Dickreuter S, Noureddine F, Bieschke P, Kern DP, Fleischer M. Self-assembled quasi-hexagonal arrays of gold nanoparticles with small gaps for surface-enhanced Raman spectroscopy. Beilstein J Nanotechnol 2018;9:1977–85.
[71] Cao Y-Q, Qin K, Zhu L, et al. Atomic-layer-deposition assisted formation of wafer-scale double-layer metal nanoparticles with tunable nanogap for surface-enhanced Raman scattering. Sci Rep 2017;7:5161.
[72] Chen X, Park H-R, Pelton M, et al. Atomic layer lithography of wafer-scale nanogap arrays for extreme confinement of electromagnetic waves. Nat Commun 2013;4:2361.
[73] Song B, Yao Y, Groenewald RE, et al. Probing gap plasmons down to subnanometer scales using collapsible nanofingers. ACS Nano 2017;11:5836–43.
[74] Im H, Bantz KC, Lindquist NC, Haynes CL, Oh S-H. Vertically oriented sub-10-nm plasmonic nanogap arrays. Nano Lett 2010;10:2231–6.

[75] Mirkin CA, Letsinger RL, Mucic RC, Storhoff JJ. A DNA-based method for rationally assembling nanoparticles into macroscopic materials. Nature 1996;382:607.
[76] Alivisatos AP, Johnsson KP, Peng X, et al. Organization of ‘nanocrystal molecules’ using DNA. Nature 1996;382:609.
[77] Fernandez YD, Sun L, Gschneidtner T, Moth-Poulsena K. Research update: progress in synthesis of nanoparticle dimers by self-assembly. APL Mater 2014;2:010702.
[78] Ciracì C, Hill RT, Mock JJ, et al. Probing the ultimate limits of plasmonic enhancement. Science 2012;337:1072–4.
[79] Tan SF, Wu L, Yang JK, Bai P, Bosman M, Nijhuis CA. Quantum Plasmon resonances controlled by molecular tunnel junctions. Science 2014;343:1496–9.
[80] Prangsma JC, Kern J, Knapp AG, et al. Electrically connected resonant optical antennas. Nano Lett 2012;12:3915–9.
[81] Carolin B, Opilik L, Atkin JM, et al. Tip-enhanced Raman spectroscopy – an interlaboratory reproducibility and comparison study. J Raman Spectrosc 2014;45:22–31.
[82] Jäger S, Kern AM, Hentschel M, et al. Au nanotip as luminescent near-field probe. Nano Lett 2013;13:3566–70.
[83] Marcus S, Stanciu C, Lieb MA, Meixner AJ. Imaging nanometre-sized hot spots on smooth Au films with high-resolution tip-enhanced luminescence and Raman near-field optical microscopy. ChemPhysChem 2008;9:316–20.
[84] Zhang R, Zhang Y, Dong ZC, et al. Chemical mapping of a single molecule by plasmon-enhanced Raman scattering. Nature 2013;498:82.
[85] Schneider NL, Schull G, Berndt R. Optical probe of quantum shot-noise reduction at a single-atom contact. Phys Rev Lett 2010;105:026601.
[86] Schull G, Néel N, Johansson P, Berndt R. Electron-plasmon and electron-electron interactions at a single atom contact. Phys Rev Lett 2009;102:057401.
[87] Johansson P, Monreal R, Apell P. Theory for light emission from a scanning tunneling microscope. Phys Rev B 1990;42:9210–3.
[88] Naik GV, Shalaev VM, Boltasseva A. Alternative plasmonic materials: beyond gold and silver. Advanced Materials 2013;25:3264–94.
[89] Berndt R, Gimzewski JK, Johansson P. Electromagnetic interactions of metallic objects in nanometer proximity. Phys Rev Lett 1993;71:3493–6.
[90] Meguro K, Sakamoto K, Arafune R, Satoh M, Ushioda S. Origin of multiple peaks in the light emission spectra of a Au(111) surface induced by the scanning tunneling microscope. Phys Rev B 2002;65:165405.
[91] Rendell RW, Scalapino DJ. Surface plasmons confined by microstructures on tunnel junctions. Phys Rev B 1981;24:3276–94.
[92] Rendell RW, Scalapino DJ, Mühlschlegel B. Role of local plasmon modes in light emission from small-particle tunnel junctions. Phys Rev Lett 1978;41:1746–50.
[93] Chen C, Bobisch CA, Ho W. Visualization of Fermi’s Golden Rule through imaging of light emission from atomic silver chains. Science 2009;325:981–5.
[94] Nazin GV, Qiu XH, Ho W. Atomic Engineering of photon emission with a scanning tunneling microscope. Phys Rev Lett 2003;90:216110.
[95] Schull G, Becker M, Berndt R. Imaging Confined electrons with plasmonic light. Phys Rev Lett 2008;101:136801.
[96] Reecht G, Scheurer F, Speisser V, Dappe YJ, Mathevet F, Schull G. Electroluminescence of a polythiophene molecular wire suspended between a metallic surface and the tip of a scanning tunneling microscope. Phys Rev Lett 2014;112:047403.
[97] Kullock R, Grimm P, Ochs M, Hecht B. Directed emission by electrically driven optical antennas. in SPIE OPTO. 2018. SPIE.
[98] Pettinger B, Domke KF, Zhang D, Schuster R, Ertl G. Direct monitoring of plasmon resonances in a tip-surface gap of varying width. Phys Rev B 2007;76:113409.
[99] Zhang D, Heinemeyer U, Stanciu C, et al. Nanoscale Spectroscopic imaging of organic semiconductor films by plasmon-polariton coupling. Phys Rev Lett 2010;104:056601.
[100] Karnetzky C, Zimmermann P, Trummer C, et al. Towards femtosecond on-chip electronics based on plasmonic hot electron nano-emitters. Nat Commun 2018;9:2471.
[101] Andre A, Theurer C, Lauth J, et al. Structure, transport and photoconductance of PbS quantum dot monolayers functionalized with a copper phthalocyanine derivative. Chem Commun 2017;53:1700–3.